# Interpretation of Polarimetric Radar Covariance Matrix for Meteorological Scatterers: Theoretical Analysis

ALEXANDER V. RYZHKOV

*Cooperative Institute for Mesoscale Meteorological Studies, University of Oklahoma, Norman, Oklahoma*

(Manuscript received 25 February 2000, in final form 20 June 2000)

ABSTRACT

A simple model of the radar scattering by atmospheric particles is used to interpret all elements of the covariance scattering matrix. The components of the covariance scattering matrix and corresponding polarimetric variables are expressed via a limited number of integral parameters that characterize distributions of sizes, shapes, and orientations of meteorological scatterers.

The co–cross-polar correlation coefficients $\rho_{xh}$ and $\rho_{xv}$ measured in the horizontal–vertical linear polarization basis are the major focus of this study. It is shown that the magnitudes of both coefficients are almost entirely determined by orientation of particles and do not depend on particle sizes and shapes. The phases of these coefficients can be used to detect the presence of melting hail or wet snow in the radar resolution volume.

A model of the mean canting angle of raindrops varying along a propagation path is developed to examine effects of propagation on the depolarization variables such as $\rho_{xh}$, $\rho_{xv}$, and linear depolarization ratio. Analysis shows that depolarization variables are very sensitive to the mean canting angle averaged over a long propagation path.

## 1. Introduction

Recently developed meteorological dual-polarization research radars can measure all components of the covariance backscattering matrix, thus exhausting all polarimetric content of the radar signal. The National Center for Atmospheric Research (NCAR's) S-Pol and Colorado State University's (CSU's) University of Chicago–University of Illinois radar (CHILL) are examples of such radars (Lutz et al. 1997; Brunkow et al. 1997). The NWS WSR-88D polarimetric upgrade is under way, and full polarimetric capability, in principle, can be implemented even for operational radar (Doviak et al. 2000). Large amounts of observational data, including all elements of the covariance scattering matrix, already exist. Recently, the NCAR S-Pol radar performed continuous weather observations in the ''full-polarization mode'' during a two-month period in Brazil within the framework of the Tropical Rainfall Measuring Mission–Large Scale Biosphere–Atmosphere Experiment (TRMM–LBA) field campaign. Appropriate interpretation of these measurements will help to further improve the algorithms for automatic hydrometeor classification originally proposed for smaller number of polarimetric variables (Straka and Zrnić 1993; Vivekanandan et al. 1999; Zrnić and Ryzhkov 1999).

According to definition, the polarimetric radar covariance matrix is composed of the second-order moments $\overline{V_{ij}}$, $\overline{V_{kl}}$, where $V_{ij}$ and $V_{kl}$ are the complex voltages in the co-polar and cross-polar receiver channels, first index specifies polarization state of a received wave, and second index stands for polarization of a transmitted wave, overbar means temporal averaging. In the absence of propagation effects, the measured (voltage) covariance matrix is a scalar multiple of the scattering covariance matrix $\mathbf{C}$ of particles filling the radar's resolution volume. The matrix $\mathbf{C}$ in the arbitrary polarization basis is defined as (Zrnić 1991)

$$\mathbf{C} = \begin{bmatrix} \langle |s_{11}|^2 \rangle & \langle s_{11}^* s_{12} \rangle & \langle s_{11}^* s_{22} \rangle \\ \langle s_{11} s_{12}^* \rangle & \langle |s_{12}|^2 \rangle & \langle s_{22} s_{12}^* \rangle \\ \langle s_{11} s_{22}^* \rangle & \langle s_{22}^* s_{12} \rangle & \langle |s_{22}|^2 \rangle \end{bmatrix}. \quad (1)$$

In (1), $s_{ij}$ means the complex scattering amplitude of an individual scatterer whereas brackets denote ensemble averaging. In the presence of propagation effects, the voltage covariance matrix is no longer a scalar multiple of $\mathbf{C}$, and their relation depends on differential attenuation, differential phase, and depolarization along the propagation path.

Extensive studies of different elements of the covariance scattering matrix in the linear or circular polarization bases and their relation to the microphysical

*Corresponding author address:* Dr. Alexander V. Ryzhkov, CIMMS/NSSL, 1313 Halley Circle, Norman, OK 73069.
E-mail: ryzhkov@nssl.noaa.gov

properties of hydrometeors started in midseventies with the pioneering works of McCormick and Hendry (1975) and Seliga and Bringi (1976). These original works paved the way for subsequent modeling and experimental studies concerning different polarimetric variables and different types of atmospheric particles including raindrops, hail, graupel, snow, and crystals (e.g., Holt 1984; Aydin and Seliga 1984; Jameson 1985, 1987; Sachidananda and Zrnić 1986; Metcalf 1988; Bringi and Hendry 1990; Vivekanandan et al. 1991; Ryzhkov 1991; Torlaschi and Holt 1993, 1998; Matrosov et al. 1996).

In the horizontal–vertical polarization basis (hereafter ''HV basis''), the diagonal terms of the scattering matrix and their ratios, such as differential reflectivity $Z_{\rm DR} = \langle|s_{hh}|^2\rangle/\langle|s_{vv}|^2\rangle$ and depolarization ratio LDR $= \langle|s_{hv}|^2\rangle/\langle|s_{hh}|^2\rangle$, have been well studied. Indexes ''$h$'' and ''$v$'' denote horizontal and vertical polarizations, respectively. The same is true for the co-polar correlation coefficient

$$\rho_{hv} = \frac{\langle s_{hh}^* s_{vv}\rangle}{(\langle|s_{hh}|^2\rangle\langle|s_{vv}|^2\rangle)^{1/2}}. \quad (2)$$

The remaining correlation coefficients,

$$\rho_{xh} = \frac{\langle s_{hh}^* s_{hv}\rangle}{(\langle|s_{hh}|^2\rangle\langle|s_{hv}|^2\rangle)^{1/2}} \quad \text{and} \quad (3)$$

$$\rho_{xv} = \frac{\langle s_{vv}^* s_{hv}\rangle}{(\langle|s_{vv}|^2\rangle\langle|s_{hv}|^2\rangle)^{1/2}}, \quad (4)$$

have been only briefly explored previously by Hendry et al. (1987) and Antar and Hendry (1987). In both papers, the authors presented some estimates of the magnitudes of $\rho_{xh}$ and $\rho_{xv}$ in rain, snow, and melting layer, but didn't mention any measurements of their phases. Examination of the coefficients $\rho_{xh}$ and $\rho_{xv}$ is one of the main focal points of this paper. The corresponding co– cross-polar correlation coefficients in the circular polarization basis were studied much more extensively. It was established that their magnitudes (ORTT in notations of McCormick and Hendry 1975) are determined by a degree of common alignment of particles, whereas their phases contain information about the mean canting angle and indicate the presence of non-Rayleigh particles in the radar resolution volume. As our recent study shows (Ryzhkov et al. 1999), the coefficients $\rho_{xh}$ and $\rho_{xv}$ are also closely related to the characteristics of hydrometeor orientation.

The polarimetric variables for the circular polarization basis are substantially affected by propagation through a medium of anisotropic scatterers. Sometimes it is very difficult to separate forward scatter and backscatter effects in radar returns for circularly (or elliptically) polarized waves. Consideration of the utility of polarimetric variables in various bases indicates that the $Z_{\rm DR}$ and $K_{\rm DP}$ (specific differential phase) are prime information carrying quantities. Measurements of the basic polarimetric variables $Z_{\rm DR}$, $K_{\rm DP}$, and $\rho_{hv}$ in the linear polarization basis are much less biased by propagation and therefore are more attractive for rainfall estimation than the variables measured in the circular polarization basis. This reasoning led to the choice of the HV basis for the future polarimetric upgrade of the operational WSR-88D radar in the U.S. radar network (Doviak et al. 2000).

There are several pressing practical issues that arose recently and prompted us to revisit earlier studies and undertake the research presented in this paper.

1) Huge amounts of data collected with linear polarization radars in the ''full-polarimetric mode'' already exist and require interpretation.
2) A number of technical questions regarding microwave circuit design, data processing, and antenna scanning strategy are being raised in support of the ongoing polarimetric upgrade of the WSR-88D radar. Some of these are listed below.
   (a) A polarimetric scheme employing simultaneous transmission (and reception) of horizontally and vertically polarized waves is suggested for the WSR-88D (Doviak et al. 2000). This approach eliminates an expensive high-power polarization switch and has other advantages. Some polarimetric variables (such as $Z_{\rm DR}$), however, can be noticeably biased under the suggested simultaneous scheme if the net (averaged over a long propagation path) canting angle of drops is substantially different from zero. Thus, any information regarding raindrop canting angles will be invaluable to assess the effectiveness of the suggested scheme.
   (b) A prospective polarimetric rainfall estimation algorithm is based on specific differential phase $K_{\rm DP}$ (either alone or in combination with radar reflectivity and differential reflectivity). If raindrops are canted, then the $K_{\rm DP}$ estimated for equioriented drops must by multiplied by the factor $\exp(-2\sigma^2)$, where $\sigma$ is the dispersion of the canting angle distribution (Oguchi 1983). This factor was always ignored in interpretation of the $K_{\rm DP}$ data because of the widespread opinion that $\sigma$ is quite small. Indeed, for $\sigma$ less than 5°, negative bias in $K_{\rm DP}$ is negligible (less than 2%), but it increases rapidly for larger $\sigma$: 6% for $\sigma = 10°$ and 13% for $\sigma = 15°$. This fact alone can explain persistent negative bias of about 10% in polarimetric rainfall estimates based on $K_{\rm DP}$ cited by two independent observational studies, one at NSSL (Ryzhkov and Zrnić 1996) and the other at NCAR (Brandes et al. 2001). Although raindrop size distribution variations or uncertainties in the drop shape are more likely causes of the observed bias, we should not ignore canting angle dispersion as a possible contributor to a resulting error.

   There is no consensus on the range of $\sigma$ in

precipitation. According to Beard and Jameson (1983), the theory predicts a mean canting angle of zero with rms values $\sigma < 4°$ for feasible turbulence intensities in the boundary layer. McCormick and Hendry (1974) reported $\sigma \approx 2°$, which is consistent with the theory of Beard and Jameson. Direct observations of individual drops near the ground in strong convection made by Saunders (1971) suggest that canting angles are symmetrically distributed about a mean of zero, with standard deviation of about 30°. Saunders' results, however, are not applicable above the surface layer. Generally, estimates of $\sigma$ from depolarization measurements on terrestrial links agree better with Saunders than with Beard and Jameson or McCormick and Hendry (Olsen 1981). Given this uncertainty, it is important to develop a reliable method for $\sigma$ estimation in the precipitation medium in order to guarantee acceptable accuracy of polarimetric radar rainfall measurements.

(c) The proposed scheme for a polarimetric WSR-88D is flexible enough to allow, along with simultaneous transmission of $H$ and $V$ waves, transmission of either $H$ or $V$ alone with simultaneous reception of both orthogonal components of the radar signal, at least for certain antenna scans. Thus, all depolarization variables [linear depolarization ratio (LDR), $\rho_{xh}$, and $\rho_{xv}$] can be, in principle, measured in addition to the basic ones obtained from the simultaneous transmission ($Z_{DR}$, $K_{DP}$, and $\rho_{hv}$). The question is how beneficial are the depolarization variables for polarimetric rainfall estimation and hydrometeor classification.

This paper is organized as follows. In section 2, general analysis of the intrinsic covariance matrix is performed for linear and circular polarizations, with special emphasis on the co-cross-polar correlation coefficients. Section 3 deals with analysis of propagation effects and their influence on the depolarized variables in the linear and circular polarization bases. A model of a nonuniform propagation path is developed that allows for continuous change of the mean canting angle. Section 4 describes possible practical implications of the $\rho_{xh}$ and $\rho_{xv}$ measurements, including estimates of the parameters of raindrop orientation and detection of non-Rayleigh scatterers such as hailstones or large wet snowflakes.

## 2. Intrinsic covariance scattering matrix of the ensemble of hydrometeors

Atmospheric particles are usually modeled as spheroids. The scattering matrix of an individual hydrometeor can be written as (Holt 1984)

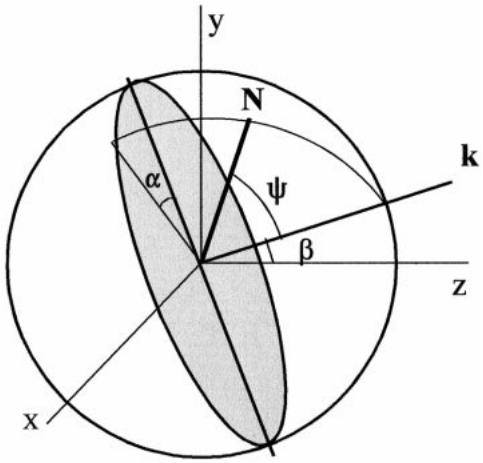


FIG. 1. Geometry of scattering. Shaded area represents polarization plane. Direction **N** denotes orientation of the symmetry axis of the particle, **k** represents the direction of wave propagation, and $y$ is the true vertical.

$$S_l = \begin{bmatrix} s_{hh} & s_{hv} \\ s_{vh} & s_{vv} \end{bmatrix} = \begin{bmatrix} s_{xx}\cos^2\alpha + s_{yy}\sin^2\alpha & (s_{yy} - s_{xx})\sin\alpha\cos\alpha \\ (s_{yy} - s_{xx})\sin\alpha\cos\alpha & s_{yy}\cos^2\alpha + s_{xx}\sin^2\alpha \end{bmatrix} \quad (5)$$

in the HV basis and

$$S_c = \begin{bmatrix} S_{rr} & S_{rl} \\ S_{lr} & s_{ll} \end{bmatrix} = \frac{1}{2}\begin{bmatrix} (s_{xx} - s_{yy})e^{-j2\alpha} & s_{xx} + s_{yy} \\ s_{xx} + s_{yy} & (s_{xx} - s_{yy})e^{j2\alpha} \end{bmatrix} \quad (6)$$

in the circular polarization basis. In (5) and (6), $s_{xx}$ and $s_{yy}$ are the scattering amplitudes and $\alpha$ is the canting angle in the polarization plane (Fig. 1). In the matrix $S_c$, index "$r$" means right-hand circular polarization, whereas index "$l$" stands for left-hand circular polarization. The scattering amplitudes $s_{xx}$ and $s_{yy}$ are generally functions of the angle $\psi$, that is, the orientation angle of the scatterer with respect to the direction of propagation **k** (Fig. 1). As was shown by Holt and Shepherd (1979), the dependence is very simple for Rayleigh scatterers (the so-called backscatter rule)

$$s_{xx} = f_b, \qquad s_{yy} = f_a \sin^2\psi + f_b \cos^2\psi, \quad (7)$$

where $f_a$ is the scattering amplitude if the electric field vector is parallel to the symmetry axis of the hydrometeor, and $f_b$ stands for the scattering amplitude if the electric vector is perpendicular to the symmetry axis. The same authors indicate that the backscatter rule holds for oblate raindrops up to 35 GHz, provided that $\psi \geq 80°$. In this paper, we deal with the polarimetric data analysis at S band, where the backscatter rule is valid for most hydrometeors except very large hail. Using (7), we can write the expressions for the matrices $S_l$ and $S_c$ as follows:

$$S_1 = \begin{bmatrix} (f_a - f_b)\sin^2\psi\sin^2\alpha + f_b & (f_a - f_b)\sin^2\psi\sin\alpha\cos\alpha \\ (f_a - f_b)\sin^2\psi\sin\alpha\cos\alpha & (f_a - f_b)\sin^2\psi\cos^2\alpha + f_b \end{bmatrix} \quad \text{and} \tag{8}$$

$$S_c = \frac{1}{2}\begin{bmatrix} (f_a - f_b)\sin^2\psi e^{-j2\alpha} & (f_a - f_b)\sin^2\psi + 2f_b \\ (f_a - f_b)\sin^2\psi + 2f_b & (f_a - f_b)\sin^2\psi e^{j2\alpha} \end{bmatrix}. \tag{9}$$

Assuming that distributions of particle orientations and particle sizes and shapes are independent and multiple scattering is insignificant, one can derive expressions for the components of the covariance scattering matrix for an ensemble of hydrometeors in the HV polarization basis (Ryzhkov 1991):

$$\begin{aligned} \langle|s_{hh}|^2\rangle_n &= 1 - 2\mathrm{Re}J_2A_2 + J_1A_4, \\ \langle|s_{vv}|^2\rangle_n &= 1 - 2\mathrm{Re}J_2A_1 + J_1A_3, \\ \langle|s_{hv}|^2\rangle_n &= \langle|s_{vh}|^2\rangle_n = J_1A_5, \\ \langle s_{hh}^* s_{vv}\rangle_n &= 1 + J_1A_5 - J_2A_1 - J_2^*A_2, \\ \langle s_{hh}^* s_{hv}\rangle_n &= \frac{1}{2}(J_1A_8 - J_2A_6), \\ \langle s_{vv}^* s_{hv}\rangle_n &= \frac{1}{2}(J_1A_7 - J_2A_6), \end{aligned} \tag{10}$$

and in the circular polarization basis:

$$\begin{aligned} \langle|s_{rr}|^2\rangle_n &= \langle|s_{ll}|^2\rangle_n = \frac{1}{4}J_1B_2, \\ \langle|s_{rl}|^2\rangle_n &= 1 - \mathrm{Re}J_2B_1 + \frac{1}{4}J_1B_2, \qquad \langle s_{rr}^* s_{ll}\rangle_n = \frac{1}{4}J_1B_5, \\ \langle s_{rr}^* s_{rl}\rangle_n &= \frac{1}{2}J_2^*B_3 - \frac{1}{4}J_1B_4, \\ \langle s_{ll}^* s_{rl}\rangle_n &= \frac{1}{2}J_2^*B_3^* - \frac{1}{4}J_1B_4^*. \end{aligned} \tag{11}$$

In formulas (10) and (11), index "$n$" in the left parts of the equations means normalization by a factor of $\langle|f_b|^2\rangle$. All normalized terms of the covariance scattering matrices are expressed through the moments,

$$J_1 = \frac{\langle|f_b - f_a|^2\rangle}{\langle|f_b|^2\rangle} \quad \text{and} \quad J_2 = \frac{\langle f_b^*(f_b - f_a)\rangle}{\langle|f_b|^2\rangle}, \tag{12}$$

which depend on size and shape distributions of particles and their refractive index, and angular moments,

$$\begin{aligned} A_1 &= \langle\sin^2\psi\cos^2\alpha\rangle, & A_2 &= \langle\sin^2\psi\sin^2\alpha\rangle, \\ A_3 &= \langle\sin^4\psi\cos^4\alpha\rangle, & A_4 &= \langle\sin^4\psi\sin^4\alpha\rangle, \\ A_5 &= \langle\sin^4\psi\cos^2\alpha\sin^2\alpha\rangle, & A_6 &= \langle\sin^2\psi\sin2\alpha\rangle, \\ A_7 &= \langle\sin^4\psi\cos^2\alpha\sin2\alpha\rangle, & A_8 &= \langle\sin^4\psi\sin^2\alpha\sin2\alpha\rangle, \\ B_1 &= \langle\sin^2\psi\rangle, & B_2 &= \langle\sin^4\psi\rangle, \\ B_3 &= \langle\sin^2\psi e^{j2\alpha}\rangle, & B_4 &= \langle\sin^4\psi e^{j2\alpha}\rangle, \\ B_5 &= \langle\sin^4\psi e^{j4\alpha}\rangle. \end{aligned} \tag{13}$$

Simple formulas can be obtained for angular moments in three special cases: (a) completely random orientation of hydrometeors, (b) random orientation in the horizontal plane, and (c) two-dimensional axisymmetric Gaussian distribution. In the latter case, the mean orientation of the hydrometeors is in the direction ($\langle\psi\rangle$, $\langle\alpha\rangle$), and the width of the angular distribution is determined by a dispersion parameter $\sigma$. The expressions for angular moments in all three cases are given in the appendix.

Using formulas (10)–(11) in these three special cases, we can easily express all measured polarimetric variables via a limited number of the moments $J_i$, $A_i$, and $B_i$ that characterize microphysical properties of meteorological scatterers. Hereafter, we will focus mainly on depolarization measurands, including depolarization ratios and co–cross-polar correlation coefficients in the linear and circular polarization bases. These variables can be measured with polarization radars capable to receive both orthogonal components of the radar signal simultaneously as well as with the radars that have one receiver but switch polarization at transmission and reception in a special manner (Zrnić 1991).

In the first two cases for which hydrometeors orient randomly either in the 3D or 2D space, the correlation coefficients, $\rho_{xh}$ and $\rho_{xv}$, for linear polarizations are zero. The corresponding coefficients,

$$\rho_{xr} = \frac{\langle s_{rr}^* s_{rl}\rangle}{(\langle|s_{rr}|^2\rangle)^{1/2}(\langle|s_{rl}|^2\rangle)^{1/2}} \quad \text{and} \tag{14}$$

$$\rho_{xl} = \frac{\langle s_{ll}^* s_{rl}\rangle}{(\langle|s_{ll}|^2\rangle)^{1/2}(\langle|s_{rl}|^2\rangle)^{1/2}}, \tag{15}$$

for circular polarization are also zero for fully random orientation of scatterers [case (a)] but differ from zero for hydrometeors randomly oriented in the horizontal plane (unless antenna elevation angle $\beta$ is equal to $\pi/2$, i.e., the radar is looking vertically).

Circular depolarization ratio (CDR), defined as

$$\mathrm{CDR} = \frac{\langle|s_{rr}|^2\rangle}{\langle|s_{rl}|^2\rangle}, \tag{16}$$

is roughly 3 dB higher than LDR if hydrometeors have

totally random orientation. For random orientation of particles in the horizontal plane, the ratio CDR/LDR is also about 3 dB for vertical sounding, but it increases with decreasing radar elevation angle (proportional to $\sin^{-2}\beta$ at low elevation angles).

The case (c) of the 2D Gaussian distribution of orientations is more interesting to examine because it represents a wide class of atmospheric scatterers, including raindrops and a large variety of frozen hydrometeors. Simple analytical formulas for angular moments and polarimetric variables can be derived for narrow angular distribution with the mean axis orientation close to vertical provided that antenna elevation angle is small. Under these assumptions, the angular moments $A_i$ and $B_i$ can be expanded in ascending powers of small parameters $\pi/2 - \langle\psi\rangle$, $\langle\alpha\rangle$, and $\sigma \approx \sigma_\alpha = \sigma/\sin\langle\psi\rangle$.

In this approximation, CDR can be expressed as

$$\mathrm{CDR} = \frac{1}{4}\frac{J_1}{\left(1 - \mathrm{Re}J_2 + \frac{1}{4}J_1\right)} = \frac{\langle|f_b - f_a|^2\rangle}{\langle|f_b + f_a|^2\rangle} \quad (17)$$

and does not depend on particle orientations. In contrast, LDR essentially depends on hydrometeor orientation, as can be inferred from (10) and (A4),

$$\mathrm{LDR} \approx J_1(\sigma^2 + \langle\alpha\rangle^2), \quad (18)$$

and the ratio

$$\frac{\mathrm{CDR}}{\mathrm{LDR}} \approx \frac{\langle|f_b|^2\rangle}{\langle|f_b + f_a|^2\rangle}\frac{1}{\sigma^2 + \langle\alpha\rangle^2} \quad (19)$$

depends primarily on characteristics of drop orientation in rain medium because the ratio $\langle|f_b|^2\rangle/\langle|f_a + f_b|^2\rangle$ varies insignificantly in rain (between 0.25 and 0.35). Thus, for small $\langle\alpha\rangle$ and $\sigma$, CDR can be significantly higher than LDR in rain (Holt et al. 1999).

Simple relations can be obtained also for co–cross-polar covariances. In the linear polarization basis, we can write the following formulas for the normalized covariances if $\alpha \ll 1$, $\pi/2 - \psi \ll 1$:

$$\langle s_{hh}^* s_{hv}\rangle_n \approx -J_2\langle\alpha\rangle = -\frac{\langle f_b^*(f_b - f_a)\rangle}{\langle|f_b|^2\rangle}\langle\alpha\rangle \quad \text{and} \quad (20a)$$

$$\langle s_{vv}^* s_{hv}\rangle_n \approx (J_1 - J_2)\langle\alpha\rangle = -\frac{\langle f_a^*(f_b - f_a)\rangle}{\langle|f_b|^2\rangle}\langle\alpha\rangle. \quad (20b)$$

Taking into account that

$$\langle|s_{hh}|^2\rangle_n \approx 1 \quad \text{and} \quad \langle|s_{vv}|^2\rangle_n \approx \frac{\langle|f_a|^2\rangle}{\langle|f_b|^2\rangle}, \quad (21)$$

and using (18), one can derive simple formulas for the correlation coefficients $\rho_{xh}$ and $\rho_{xv}$:

$$\rho_{xh,xv} = b_{h,v}\frac{\langle\alpha\rangle}{(\sigma^2 + \langle\alpha\rangle^2)^{1/2}}, \quad (22)$$

where

$$b_{h,v} = -\frac{\langle f_{b,a}^*(f_b - f_a)\rangle}{\langle|f_{b,a}|^2\rangle^{1/2}\langle|f_b - f_a|^2\rangle^{1/2}}. \quad (23)$$

The coefficients $b_h$ and $b_v$ do not vary much in rain. In order to estimate their variations, we have used simulated Gamma drop size distributions

$$N(D) = N_0 D^m \exp\left(-\frac{(3.67 + m)D}{D_0}\right), \quad (24)$$

with parameters $m$ and $D_0$ within the ranges ($-1$ to 4) and (0.5–2.5 mm), respectively, as was recommended by Ulbrich (1983). We also assume the Pruppacher–Pitter dependence of the drop oblateness on its equivolume diameter (Pruppacher–Pitter 1971). The coefficients $b_h$ and $b_v$ do not depend on the total drop concentration $N_0$. Simulations show that $b_h$ varies mainly within the interval 0.85–0.95, whereas $b_v$ changes from 0.80 to 0.90. Thus, the co–cross-polar correlation coefficients for linear polarizations are determined almost entirely by the parameters $\langle\alpha\rangle$ and $\sigma$ of the angular distribution of scatterers. If the dispersion $\sigma$ is larger than the mean canting angle $\langle\alpha\rangle$, then the magnitudes of $\rho_{xh}$ and $\rho_{xv}$ are roughly proportional to the ratio $|\langle\alpha\rangle|/\sigma$.

For Rayleigh scatterers with small imaginary parts of refractive index, like crystals or dry snowflakes, the arguments of $b_h$ and $b_v$ are close to zero, and the phase of both coefficients $\rho_{xh}$ and $\rho_{xv}$ is either 0 or $\pi$, depending on the sign of the mean canting angle. For Rayleigh scatterers with larger imaginary parts of refractive index or non-Rayleigh particles, the arguments of $b_h$ and $b_v$ differ from zero and contain important information about microphysical properties of hydrometeors. More detailed discussion of this matter is in section 4.

In the circular polarization basis, the covariances $\langle s_{rr}^* s_{rl}\rangle_n$ and $\langle s_{ll}^* s_{rl}\rangle_n$ can be written as

$$\langle s_{rr}^* s_{rl}\rangle_n = \frac{1}{2}(J_2^* - J_1)(1 - 2\sigma^2)e^{-2j\langle\alpha\rangle},$$

$$\langle s_{ll}^* s_{rl}\rangle_n = \frac{1}{2}(J_2^* - J_1)(1 - 2\sigma^2)e^{2j\langle\alpha\rangle}, \quad (25)$$

and the coefficients $\rho_{xr}$ and $\rho_{xl}$ can be expressed in the following form:

$$\rho_{xr} = b_c(1 - 2\sigma^2)e^{-j2\langle\alpha\rangle} \quad \text{and}$$

$$\rho_{xl} = b_c(1 - 2\sigma^2)e^{j2\langle\alpha\rangle}, \quad (26)$$

where

$$b_c = \frac{\langle(f_b + f_a)(f_b^* - f_a^*)\rangle}{\langle|f_b + f_a|^2\rangle^{1/2}\langle|f_b - f_a|^2\rangle^{1/2}}. \quad (27)$$

Analysis of the factor $b_c$ shows that for all simulated drop size distributions (DSDs) $|b_v| < |b_c| < |b_h|$. The magnitudes of $\rho_{xr}$ and $\rho_{xl}$ [ORTT in the notations of McCormick and Hendry (1975)] do not depend on the mean canting angle and are affected by the dispersion

of the canting angle distribution $\sigma$. In rain medium, ORTT is almost equally affected by variations of DSD via parameter $b_c$ and changes in the orientations of scatterers through parameter $\sigma$. Hence in rain, ORTT, strictly speaking, is not a measure of a degree of common alignment of drops. This was first pointed out by Holt (1984). ''Linear ORTT,'' that is, the magnitude of $\rho_{xh}$ or $\rho_{xv}$, is much more sensitive to the changes in raindrops orientation than to the DSD variations.

Another difference between the co–cross-polar correlation coefficients in the HV and circular polarization bases is in their phases. The phases of $\rho_{xr}$ and $\rho_{xl}$ are determined by the mean canting angle (its absolute value and a sign) and the argument of $b_c$ that is different from zero for non-Rayleigh scatterers or for the scatterers with large imaginary parts of refractive index. In contrast, the phase of $\rho_{xh,xv}$ is sensitive only to the sign of the mean canting angle. Any difference of the $\arg(\rho_{xh,xv})$ from 0 or $\pm\pi$ is attributed to the $\arg(b_{h,v})$ that is very close to the $\arg(b_c)$. This simple interpretation is valid only in the absence of propagation effects, as will be shown in the next section.

## 3. Effects of propagation

Depending on polarization and propagation direction, electromagnetic (EM) waves in anisotropic media of canted hydrometeors can experience differential attenuation, differential phase shift, and depolarization. Therefore, the polarization state of EM wave is continuously changing as it propagates in the anisotropic medium. This change is described via the transmission matrix $\mathbf{T}$, and the intrinsic backscattering matrix $\mathbf{S}$ for an individual hydrometeor is transformed into the matrix $\mathbf{S}' = \mathbf{T}^{\mathrm{T}}\mathbf{S}\mathbf{T}$, where superscript T means transposition. The transmission matrix $\mathbf{T}$ has a simple form for uniform propagation path:

$$\mathbf{T}_l = \begin{bmatrix} d_x \cos^2\theta + d_y \sin^2\theta & (d_y - d_x)\sin\theta\cos\theta \\ (d_y - d_x)\sin\theta\cos\theta & d_x \sin^2\theta + d_y \cos^2\theta \end{bmatrix} \tag{28}$$

in the HV polarization basis and

$$\mathbf{T}_c = \frac{1}{2}\begin{bmatrix} d_x + d_y & (d_x - d_y)e^{j2\theta} \\ (d_x - d_y)e^{-j2\theta} & d_x + d_y \end{bmatrix} \tag{29}$$

in the circular polarization basis. In (28) and (29), $\theta$ designates the mean canting angle of scatterers along propagation path, $d_{x,y} = \exp(-j\gamma_{x,y}R)$ are propagation factors in the two orthogonal principal planes, and $R$ is the distance from the radar. The differences between propagation constants in the two principal planes relate to differential phase $\Phi_{\mathrm{DP}}$ and differential attenuation $\Delta A$:

$$\Phi_{\mathrm{DP}} = 2\mathrm{Re}(\gamma_x - \gamma_y)R$$
$$\Delta A = -2\mathrm{Im}(\gamma_x - \gamma_y)R \tag{30}$$

If we assume that all scatterers are equioriented, that is, the canting angle in the radar resolution volume is the same as that along the preceding propagation path ($\alpha = \theta$) and $\sigma = 0$, then taking into account propagation effect is equivalent to multiplying the scattering amplitudes $s_{xx}$ and $s_{yy}$ in (5) and (6) by the factors $d_x^2$ and $d_y^2$, respectively (Holt 1984; Torlaschi and Holt 1993, 1998).

If the mean canting angle along propagation path $\theta$ is equal to zero, then the transmission matrix $\mathbf{T}_l$ in the linear polarization basis is diagonal, and no depolarization due to propagation occurs. In this situation, all intrinsic polarimetric variables are affected by propagation in a very simple and straightforward way:

$$Z'_{\mathrm{DR}}\ (\mathrm{dB}) = Z_{\mathrm{DR}}\ (\mathrm{dB}) - \Delta A\ (\mathrm{dB}),$$
$$\mathrm{LDR}'\ (\mathrm{dB}) = \mathrm{LDR}\ (\mathrm{dB}) + \frac{1}{2}\Delta A\ (\mathrm{dB}),$$
$$\rho'_{hv} = \rho_{hv}e^{j\Phi_{\mathrm{DP}}}, \qquad \rho'_{xh} = \rho_{xh}e^{j(\Phi_{\mathrm{DP}}/2)},$$
$$\rho'_{xv} = \rho_{xv}e^{-j(\Phi_{\mathrm{DP}}/2)}. \tag{31}$$

In (31), prime superscript denotes measurands in the presence of propagation effects. If the mean canting angle $\langle\alpha\rangle$ in the radar resolution volume is also equal to zero, then both $\rho_{xh}$ and $\rho_{xv}$ are identically zeros. In the circular polarization basis, substantial depolarization due to propagation takes place regardless of the mean canting angle $\theta$. This causes dramatic changes in CDR, $\rho_{xr}$, and $\rho_{xl}$ as the EM wave progresses through the uniform anisotropic medium. Figure 2 illustrates these changes as a function of differential phase $\Phi_{\mathrm{DP}}$ for $\theta = 0°$ and of uniform rain with the intensity $R$ of 30 mm $\mathrm{h}^{-1}$. Hereafter, in this section, we will make computations for $R = 30$ mm $\mathrm{h}^{-1}$ assuming that drop size distribution is Marshall–Palmer, raindrop shape factor is Pruppacher–Pitter, and

$$\Delta A\ \ (\mathrm{dB}) = 0.0035\Phi_{\mathrm{DP}}\ \ (\mathrm{deg}) \tag{32}$$

at the wavelength of 10 cm (Bringi et al. 1990).

Canted hydrometeors cause depolarization of linearly polarized $H$ and $V$ waves. If the canting angle $\theta$ is of the order of a few degrees, then the effect of depolarization on co-polar variables such as $Z_{\mathrm{DR}}$ and $\rho_{hv}$ is negligible. It is noticeable, however, in the LDR (Fig. 3a) and significant as far as co–cross-polar correlation coefficients $\rho_{xh}$ and $\rho_{xv}$ are concerned (Figs. 3b,c). Even for a small canting angle $\theta = -1°$, the magnitudes of $\rho_{xh}$ and $\rho_{xv}$ change 6 times for the rain rate 30 mm $\mathrm{h}^{-1}$ as differential phase increases from 0 to 180°. The corresponding change in the phase of $\rho_{xh}$ and $\rho_{xv}$ (after subtracting $\pm\Phi_{\mathrm{DP}}/2$) is 90° for the same $\Phi_{\mathrm{DP}}$ span. High sensitivity of $\rho_{xh}$ and $\rho_{xv}$ to depolarization along propagation paths in precipitation was first mentioned by Hubbert et al. (1999). Any visible trend in the magnitudes of $\rho_{xh}$ and $\rho_{xv}$ with distance is an indication of either nonzero net canting angle or system imperfections like feed horn misalignment, nonorthogonality of trans-

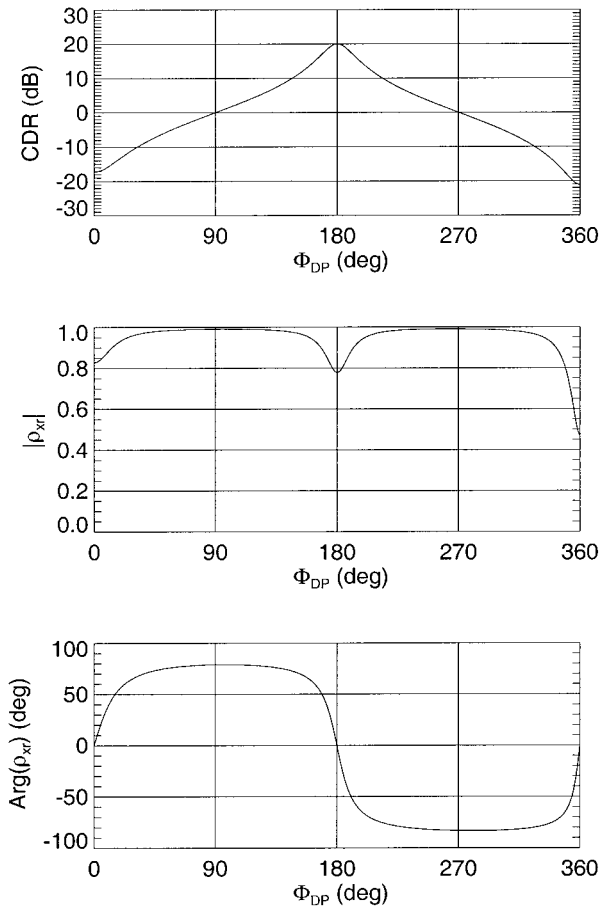


FIG. 2. Dependencies of CDR, $|\rho_{xr}|$, and $\arg(\rho_{xr})$ on differential phase $\Phi_{DP}$ for uniform precipitation with rain rate 30 mm $h^{-1}$, $\theta = 0°$, and $\sigma = 10°$. Here, as in the following Figs. 3–5, we use unprimed notations to designate polarimetric variables affected by propagation effects (CDR instead of CDR′) as opposed to notations in formulas (31).

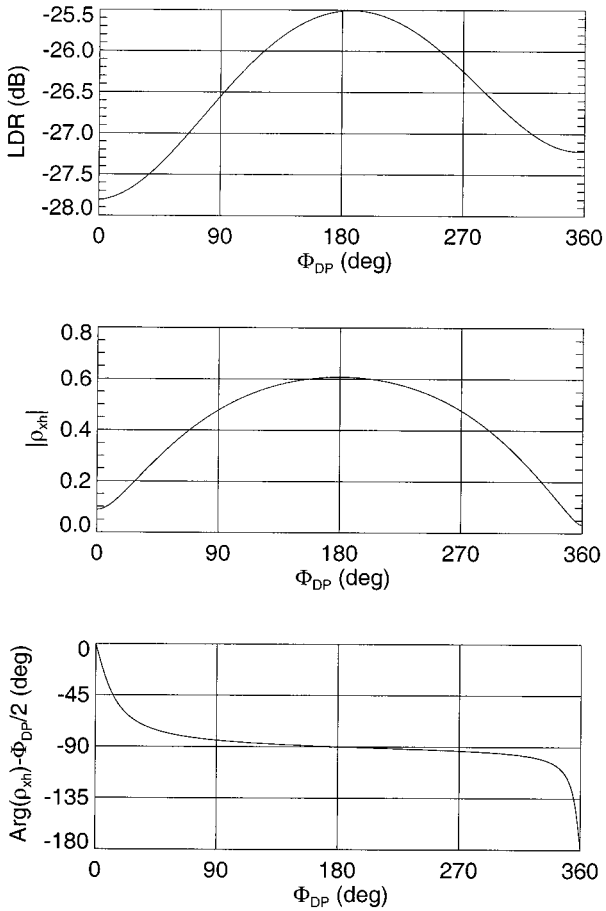


FIG. 3. Dependencies of LDR, $|\rho_{xh}|$, and $\arg(\rho_{xh}) - \Phi_{DP}/2$ on differential phase $\Psi_{DP}$ for uniform precipitation with rain rate 30 mm $h^{-1}$, $\theta = -1°$, and $\sigma = 10°$.

mitted/received waves, etc. Therefore, analysis of the $|\rho_{xh}|$ and $|\rho_{xv}|$ trends on long propagation paths through precipitation can serve as a quality check for dual-polarization radar antenna assembly and as a means to validate the simultaneous transmission scheme. All polarimetric measurands in the circular polarization basis are much less sensitive to minor variations of the mean canting angle around zero and cannot serve that purpose.

Our observations described in (Ryzhkov et al. 2000) do not reveal such pronounced trends in $|\rho_{xh}|$ and $|\rho_{xv}|$, as shown in Fig. 3 for the data collected with the S-Pol radar. This indicates that in reality, the mean canting angle averaged over a long distance in rain is very close to zero, and depolarization due to propagation is quite insignificant for the HV basis. This does not exclude, of course, that the mean canting angle in each radar resolution volume can considerably differ from zero, which manifests itself in essentially nonzero values of $|\rho_{xh}|$ and $|\rho_{xv}|$ observed in rain (Ryzhkov et al. 1999, 2000). Bearing this in mind, we believe that the model of the mean canting angle varying randomly around zero is more adequate to describe the propagation process in rain than the model with a constant nonzero canting angle.

In our model, we assume that the mean canting angle $\langle\alpha\rangle$ is a random function of range (or differential phase), with modulation that represents a slowly varying net canting angle component $\theta$. The transmission matrix for the nonuniform propagation path with varying angle $\theta$ can be constructed as a product of transmission matrices related to small range bins (gates) within which propagation medium can be considered uniform. Figure 4 represents the results of such simulation. It was assumed that the rms width of the mean canting angle distribution $\sigma_\theta$ is 2°. Note that $\sigma_\theta$ is different from $\sigma$ or $\sigma_\alpha$, which signify the rms width of the canting angle distribution within radar resolution volume (assumed to be 10° in our model computations). In Fig. 4b, where $|\rho_{xh}|$ is plotted, the corresponding curve for circular ORTT ($|\rho_{xr}|$) is also shown. The major difference between the linear ORTT ($|\rho_{xh}|$ or $|\rho_{xv}|$) and circular ORTT is that the former is very noisy but unbiased whereas the latter is

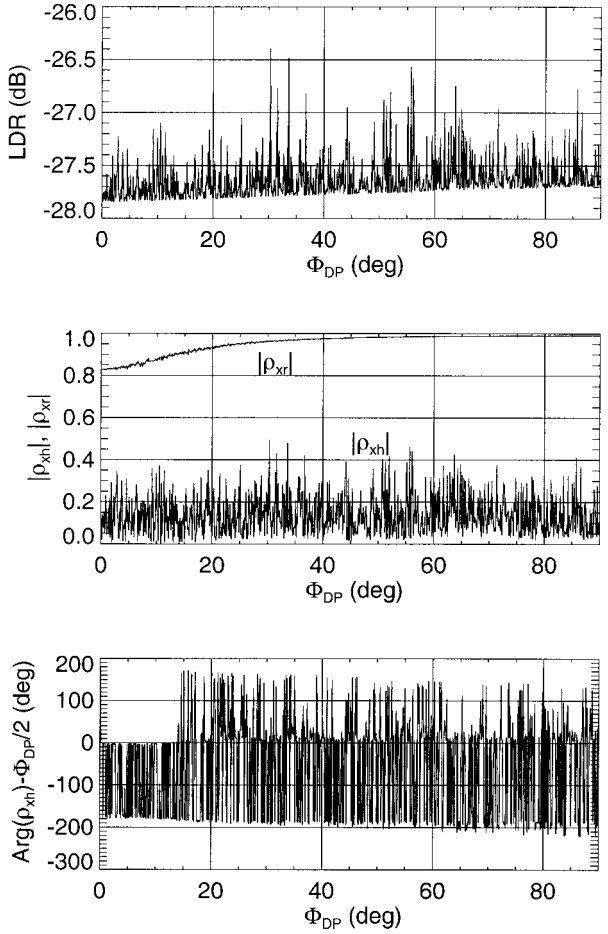


FIG. 4. Dependencies of LDR, $|\rho_{xh}|$, $|\rho_{xr}|$, and $\arg(\rho_{xh}) - \Phi_{DP}/2$ on differential phase $\Phi_{DP}$ for uniform precipitation with rain rate 30 mm $h^{-1}$, $\sigma = 10°$, and random fluctuations of the mean canting angle $\langle\alpha\rangle$ around zero with the rms value of 2°.

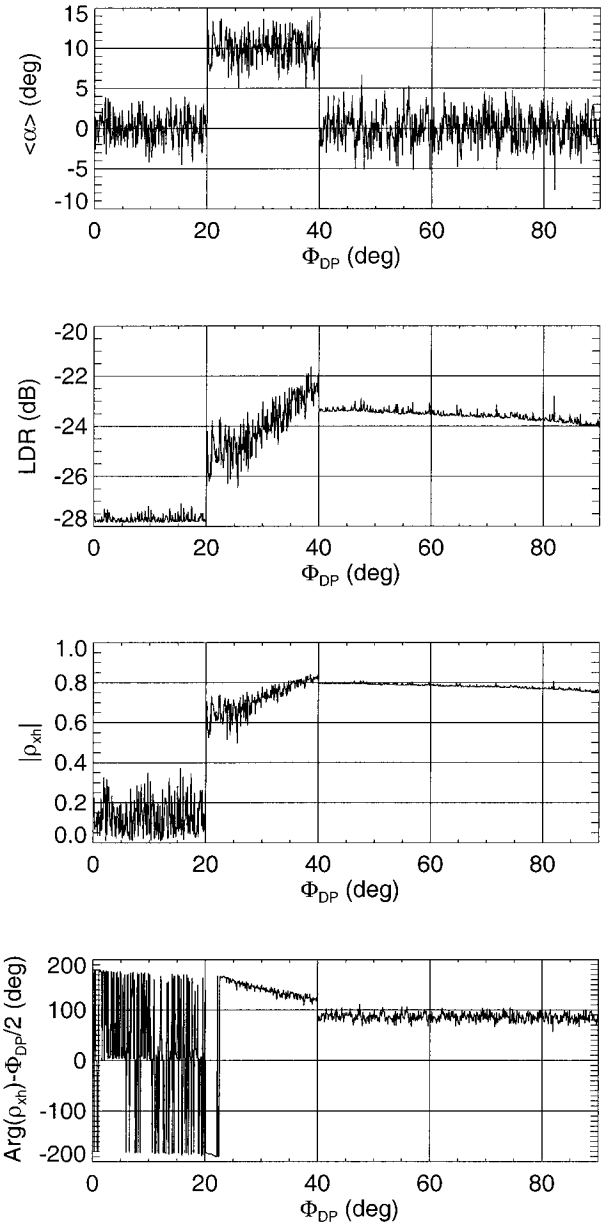


FIG. 5. Same as in Fig. 4 but $\langle\alpha\rangle = 10°$ within the interval $20° < \Phi_{DP} < 40°$.

much less noisy but biased by propagation. Extra noise in unbiased data can be eliminated by appropriate spatial and temporal averaging whereas elimination of bias due to propagation requires tricky procedures that are vulnerable to measurement errors (see, e.g., Torlaschi and Holt 1993). The behavior of the arguments of $\rho_{xh}$ ($\rho_{xv}$) changes dramatically as we allow random changes of the mean canting angle sign. The phase becomes very noisy and difficult to interpret. Along with the values of 0 and $\pm\pi$ expected in the absence of propagation, there are many intermediate values in the interval between $-\pi$ and $\pi$, which are attributed to propagation effects. The $\pm\Phi_{DP}/2$ is superposed to these values as predicted by (31).

Finally, we examine a model of a step change of the mean canting angle $\theta$ along a radial from 0° to 10° and back to 0°, with a random oscillations superimposed on it. The parameters of the random component of the mean canting angle are the same as in the previous example in Fig. 4. This type of rapid change of the mean canting angle along the radial could occur if a radar beam intercepts precipitation below the melting level and crosses the region of canted crystals at higher altitudes. Crystal orientation that is different from horizontal or vertical direction may be attributed to the presence of strong electric fields in the charged regions of thunderstorms (Caylor and Chandrasekar 1996; Krehbiel et al. 1996).

The results of simulation for this model are presented in Fig. 5. The jump of the mean canting angle at $\Phi_{DP} = 20°$ is accompanied by sharp increase of LDR and $|\rho_{xh}|$ or $|\rho_{xv}|$, according to formulas (18) and (22). Further increase of LDR and $|\rho_{xh}|$ or $|\rho_{xv}|$ with distance is caused by depolarization due to propagation because of an es-

sentially nonzero value of $\theta$. This increase is roughly proportional to the product of $\sin 2\theta \Delta\Phi_{DP}$, where $\Delta\Phi_{DP}$ is the differential phase increment within the ''crystal'' region with $\theta = 10°$. Interestingly, random fluctuations of LDR and $|\rho_{xh}|$ or $|\rho_{xv}|$ caused by oscillations of the mean canting angle decrease as the EM wave penetrates deeper into the crystal region of high depolarization. This is because depolarization propagation effects are accumulated with distance and eventually dump oscillations inherent to intrinsic LDR and $|\rho_{xh}|$ or $|\rho_{xv}|$. The phase of the co–cross-polar correlation coefficients is very noisy in the ''rain'' region, where the mean canting angle fluctuates around zero and is much more stable in the crystal region where it does not change its sign. The change of the pattern, however, does not coincide with the change of the deterministic component in $\langle\alpha\rangle$ but occurs with some delay, apparently, due to effects of propagation. When the mean canting angle returns to its initial value of 0° after $\Phi_{DP} = 40°$, all depolarization variables do not restore their initial values and patterns that characterize the rain region $0° < \Phi_{DP} < 20°$. Instead, they generally continue to retain their values acquired at the end of the ''crystal'' interval, that is, $\Phi_{DP} = 40°$, with slight tendency of LDR and $|\rho_{xh}|$ to decrease. This model, although very idealistic, reproduces quite well the patterns of LDR and $|\rho_{xh}|$ measured with the S-Pol and CHILL radars (Ryzhkov et al. 2000).

## 4. Possible practical applications of the co–cross-polar correlation coefficients

### *a. Estimation of $|\langle\alpha\rangle|$ and $\sigma$*

As it follows from the previous sections, the magnitudes of the co–cross-polar correlation coefficients in the linear polarization basis $\rho_{xh}$ and $\rho_{xv}$ are directly related to the absolute value of the mean canting angle $|\langle\alpha\rangle|$ and the rms width of the canting angle distribution $\sigma$, while their phases contain information about the sign of the mean canting angle and the presence of non-Rayleigh scatterers.

Propagation effects do not bias $|\rho_{xh}|$ and $|\rho_{xv}|$ provided that the net canting angle along the propagation path is close to zero, which is probably the case for rain medium. The angular parameters $|\langle\alpha\rangle|$ and $\sigma$ are entangled in the formula (22) for $\rho_{xh,xv}$, and thus an additional relation is required to separate $|\langle\alpha\rangle|$ and $\sigma$. It can be shown, using (10) and (A4), that $|\langle\alpha\rangle|$ can be found independently from the following relation:

$$\frac{1}{2}|\langle \sin 2\alpha\rangle| \approx |\langle\alpha\rangle| \approx \frac{2|\langle s_{hh}^* s_{hv}\rangle_n|}{\langle|s_{hh}|^2\rangle_n - \langle|s_{vv}|^2\rangle_n} = \frac{2|\rho_{xh}|(\mathrm{LDR})^{1/2}}{1 - Z_{DR}^{-1}}. \quad (33)$$

By combining (33) with (22), we can estimate $|\langle\alpha\rangle|$ and $\sigma$ separately. Strictly speaking, the formula (22) is valid only for small (less than 5°–6°) values of $|\langle\alpha\rangle|$ and $\sigma$. As our estimates from the data show (Ryzhkov et al. 1999, 2000), the magnitude of the mean canting angle in rain is indeed rather small whereas the parameter $\sigma$ can be much larger, reaching 20° or 30° in some cases. Therefore, we can expand the angular moments $A_i$ in a Taylor series using small parameters $\langle\alpha\rangle$ and $\pi/2 - \langle\psi\rangle$ but not $\sigma$ or $\sigma_\alpha$. In other words, we cannot expand $r = \exp(-2\sigma^2)$ and $r_\alpha = \exp(-2\sigma_\alpha^2)$ in the series of $\sigma^2$ and $\sigma_\alpha^2$ and retain only the first few terms. More accurate expression for $|\rho_{xh}|$ can be written as

$$|\rho_{xh}| \approx |b_h| \frac{\sqrt{2} r_\alpha |\sin 2\langle\alpha\rangle|}{\sqrt{1 - r_\alpha^4 \cos 4\langle\alpha\rangle}}, \quad (34)$$

where $r_\alpha = \exp(-2\sigma_\alpha^2)$. Here again we assume, as in (22), that $\langle\sin^2\psi\rangle \approx \langle\sin^4\psi\rangle \approx 1$ because all polarimetric variables are much less sensitive to the details of angular distribution with respect to $\psi$ than to $\alpha$ - canting angle projection on the polarization plane but do not restrict the derivation to very small values of $\sigma_\alpha$. The magnitude of the mean canting angle $|\langle\alpha\rangle|$ can be found from (33) and then inserted into (34) to obtain the estimate of the parameter $r_\alpha$ and, hence, $\sigma_\alpha$. For the factor $|b_h|$, its mean value determined by the DSD variations can be used.

Next, we examine the stability of the suggested approximate relations (33) and (34) to the expected variations of the moments $J_1$ and $J_2$ as well as to the parameters of the 2D Gaussian angular distribution $\langle\alpha\rangle$, $\langle\psi\rangle$ and $\sigma$. In order to check the relation (33), we fix the value of angle $\langle\alpha\rangle$ and allow $J_1$ and $J_2$ to change according to the DSD variations determined by the Ulbrich's parameterization, angle $\langle\psi\rangle$ to vary within the interval 84°–96°, and the rms width $\sigma$ to vary between 0° and 30°. Then we compute all polarimetric variables on the right side of Eq. (33) using (10) and (A4) and obtain the estimate of $|\langle\alpha\rangle|$ for each combination of the parameters $J_1$, $J_2$, $\langle\psi\rangle$, $\langle\alpha\rangle$, and $\sigma$ from (33). For each combination of the mentioned parameters, the estimate of $|\langle\alpha\rangle|$ given by (33) is slightly different for the fixed value of $|\langle\alpha\rangle|$. As a next step, we find its mean value and standard deviation and compare with the actual value of $|\langle\alpha\rangle|$. Then, the coefficient of proportionality in (33) (originally set to 2) is adjusted to minimize the bias of the estimate. Finally, we come up with the corrected formula

$$|\langle\alpha\rangle| = 1.87 \frac{|\rho_{xh}|(\mathrm{LDR})^{1/2}}{1 - Z_{DR}^{-1}}, \quad (35)$$

which gives us almost an unbiased estimate of the magnitude of the mean canting angle in the polarization plane within the range of 0°–6°. The fractional standard deviation of the estimate is about 5% (Fig. 6a). The same simulation procedure was applied to the estimate of $\sigma_\alpha$ from (34). In the latter case, the value of $\sigma_\alpha$ is fixed while $J_1$, $J_2$, $\langle\psi\rangle$, and $\langle\alpha\rangle$ vary. The estimate of $|\langle\alpha\rangle|$ is obtained from (35), and $r_\alpha(\sigma_\alpha)$ is computed using (34). Our simulations show that the relation

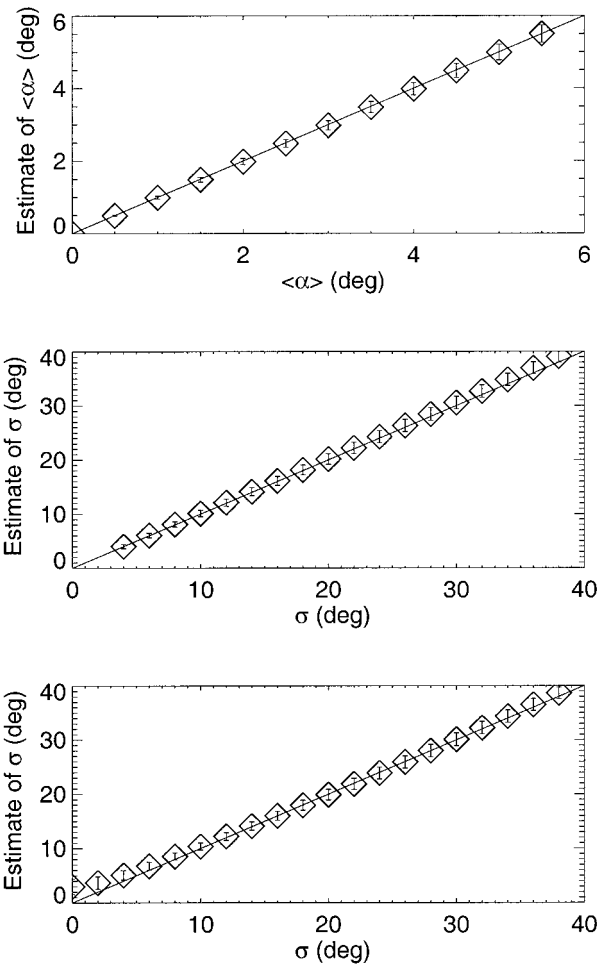


FIG. 6. (a) The estimate of $\langle\alpha\rangle$ obtained from (35) vs actual value of $\langle\alpha\rangle$, (b) the estimate of $\sigma$ obtained from (36) vs actual value of $\sigma$, (c) the estimate of $\sigma$ obtained from (37) vs actual value of $\sigma$. Vertical bars indicate the magnitude of the standard deviation of the estimate.

$$|\rho_{xh}| = 1.23\frac{r_\alpha|\sin 2\langle\alpha\rangle|}{\sqrt{1 - r_\alpha^4\cos 4\langle\alpha\rangle}}, \tag{36}$$

derived from (34) after substituting $|b_h| = 0.87$, works best of all when combined with (35). The performance of the suggested algorithm is illustrated by Fig. 6b, where the mean of the $\sigma_\alpha$ estimate and its standard deviation are displayed. The algorithm yields practically an unbiased estimate of $\sigma_\alpha$ up to 30° with the standard deviation of about 3%–7%. Note that the standard errors of the $|\langle\alpha\rangle|$ and $\sigma_\alpha$ estimates shown in Figs. 6a and 6b characterize the method itself in the absence of any measurement errors, which we do not consider in this paper.

The estimate of the parameter $\sigma_\alpha$ can be made without using $|\rho_{xh}|$ if $|\langle\alpha\rangle| \ll \sigma_\alpha$ (that is very likely the case in rain, the melting layer, or hail). It can be shown from (10) and (A4) that the ratio $(\mathrm{LDR})^{1/2}/(1 - Z_{\mathrm{DR}}^{-1})$ is almost entirely determined by the parameter $r_\alpha = \exp(-2\sigma_\alpha^2)$ provided that $|\langle\alpha\rangle| \ll \sigma_\alpha$. Using simulations similar to the ones that lead to the algorithms (35) and (36), we come up with the relation

$$\frac{\mathrm{LDR}}{(1 - Z_{\mathrm{DR}}^{-1})^2} = 0.05\frac{1 - r_\alpha^4}{r_\alpha^2} \tag{37}$$

from which the parameter $r_\alpha$ (and subsequently $\sigma_\alpha$) can be derived. The performance of this formula is illustrated by Fig. 6c, where the estimates of $\sigma_\alpha$ are plotted against the actual values of $\sigma_\alpha$. The method yields almost unbiased estimates of $\sigma_\alpha$ for $\sigma_\alpha > 8°$.

### *b. Possible detection of melting hail and wet snow using the phase of the co–cross-polar correlation coefficients*

As was shown in section 2, in the absence of propagation effects, the phases of the co–cross-polar correlation coefficients $\rho_{xh}$ and $\rho_{xv}$ in the HV basis are determined by the sign of the mean canting angle and the arguments of the complex factors $b_h$ and $b_v$ [see formula (22)]. The arguments of $b_h$ and $b_v$ are very similar to the argument of the factor $b_c$ in Eq. (26) for the co–cross-polar correlation coefficients $\rho_{xr}$ and $\rho_{xl}$ in the circular polarization basis. The phase of $b_c$ was briefly examined in some earlier studies (see, e.g., McCormick and Hendry 1975). It was shown that a large nonzero value of the argument of $b_c$ is a distinguishing property of non-Rayleigh scatterers. Examination of this non-Rayleigh component in the phase of $\rho_{xr}$ ($\rho_{xl}$), which we will call ''depolarization phase,'' did not receive further development in later works, probably because of difficulties in isolating this component from the others relating to the mean canting angle and propagation effects. Instead, more efforts were devoted to the study of the backscatter differential phase $\delta$, that is, the phase of the co-polar correlation coefficient $\rho_{hv}$ measured in the HV polarization basis. Nonzero values of $\delta$ are also indicative of the presence of non-Rayleigh scatterers and thus can be used, in principle, to delineate the areas of large hail within the storm (Balakrishnan and Zrnić 1990). The problem is that $\delta$ tends to zero for randomly oriented scatterers, which is usually the case for tumbling hailstones. The advantage of the depolarization phase is that it doesn't depend on the degree of hydrometeor common alignment. There are several other advantages that will be discussed later.

To compare the properties of the backscatter differential phase and depolarization phase, we will use the following notations for different phases that are examined in this paper: $\delta_{co} = \delta$, $\delta_{cr}^{(h)} = \arg(b_h)$, $\delta_{cr}^{(v)} = \arg(b_v)$, and $\delta_{cr}^{(c)} = \arg(b_c)$, where $b_h$, $b_v$, $b_c$ are defined by (23) and (27). For spheroidal scatterers with the axis of rotation oriented vertically,

$$\delta_{co} = \arg(f_b^* f_a) = \arg(f_a) - \arg(f_b). \tag{38}$$

It follows from (23) and (27) that for monodispersed size distribution of oblate spheroids,

$$\delta_{cr}^{(h)} = \arg(f_b - f_a) - \arg(f_b),$$
$$\delta_{cr}^{(v)} = \arg(f_b - f_a) - \arg(f_a),$$
$$\delta_{cr}^{(c)} = -\arg(f_b - f_a) + \arg(f_a + f_b). \quad (39)$$

Our computations of the complex scattering amplitudes $f_{a,b}$ for raindrops made at S, C, and X microwave frequency bands using a **T**-matrix algorithm show that both the backscatter differential phase in (38) and depolarization phases in (39) are very close to zero in the Rayleigh region of raindrop sizes. Their difference from zero does not exceed 1.5° at S band (radar wavelength $\lambda = 10$ cm) for raindrops with equivolume diameter $D_e$ below 6 mm, 3° at C band ($\lambda = 5.5$ cm) for drops with $D_e < 4$ mm, and 5° at X band ($\lambda = 3.2$ cm) for $D_e < 2.5$ mm in the wide range of water temperatures between −20° and 30°C. The magnitudes of all phases in (38) and (39) increase with decreasing temperatures but remain within indicated limits at the zero vicinity for the Rayleigh regime of scattering. In the Mie region of scattering, all the phases may exceed those limits, but the contribution of larger drops to the total backscatter differential or depolarization phase is usually rather insignificant due to a relatively small concentration of larger drops. However, melting hailstones or giant raindrops with ice cores generated from melting hail can contribute much more to the measured phase because of their larger size.

We model melting hailstones as oblate spheroids with a refractive index of water at the temperature of 0°. Since there is no established relation between hail size and oblateness, we made computations for different aspect ratios ranging from 0.80 to 0.95 and assumed, for the sake of simplicity, that they do not change with size. It was found that generally $|\delta_{cr}^{(h)}| < |\delta_{cr}^{(c)}| < |\delta_{cr}^{(v)}|$, and the ratio $|\delta_{cr}^{(v)}|/|\delta_{cr}^{(h)}|$ varies between 1.05 and 1.50, depending on oblateness. For more spherical particles, this ratio is more close to unity. It was also shown that the average of $\delta_{cr}^{(h)}$ and $\delta_{cr}^{(v)}$, namely $\delta_{cr} = \frac{1}{2}(\delta_{cr}^{(h)} + \delta_{cr}^{(v)})$, is very close to $-\delta_{cr}^{(c)}$ [as can be seen from (39)]. The results of calculations of $\delta_{co}$ and $\delta_{cr}$ for S, C, and X bands are presented in Fig. 7 for aspect ratios 0.8, 0.9, and 0.95.

Two important conclusions can be drawn from Fig. 7. First, for the aspect ratios considered, the depolarization phase $\delta_{cr}$ is much larger than the backscatter differential phase $\delta_{co}$. Second, $\delta_{co}$ essentially depends on the aspect ratio whereas $\delta_{cr}$ is almost independent of particle shape (at least in the region where $\delta_{cr}$ is positive). This striking difference between $\delta_{co}$ and $\delta_{cr}$ can be explained by the fact that the backscatter differential phase is a difference between the arguments of the complex scattering amplitudes $f_a$ and $f_b$, while the depolarization phase is determined mainly by the argument of the difference $(f_b - f_a)$ [see formulas (39)]. For all atmospheric scatterers in the microwave frequency band $|\mathrm{Re}(f_{a,b})| \gg |\mathrm{Im}(f_{a,b})|$ (even in the Mie regime of scattering). Therefore, the arguments of $f_a$ and $f_b$ as well as their differences are quite small. In contrast, the ratio $|\mathrm{Im}(f_b - f_a)|/|\mathrm{Re}(f_b - f_a)|$, which determines the depolarization phase, is not necessarily very small, especially if $f_a \approx f_b$, that is, for nearly spherical hydrometeors. Of course, the scatterers must be nonspherical enough to produce a tangible depolarization component in the reflected EM field so that the co–cross-polar correlation coefficients can be measured.

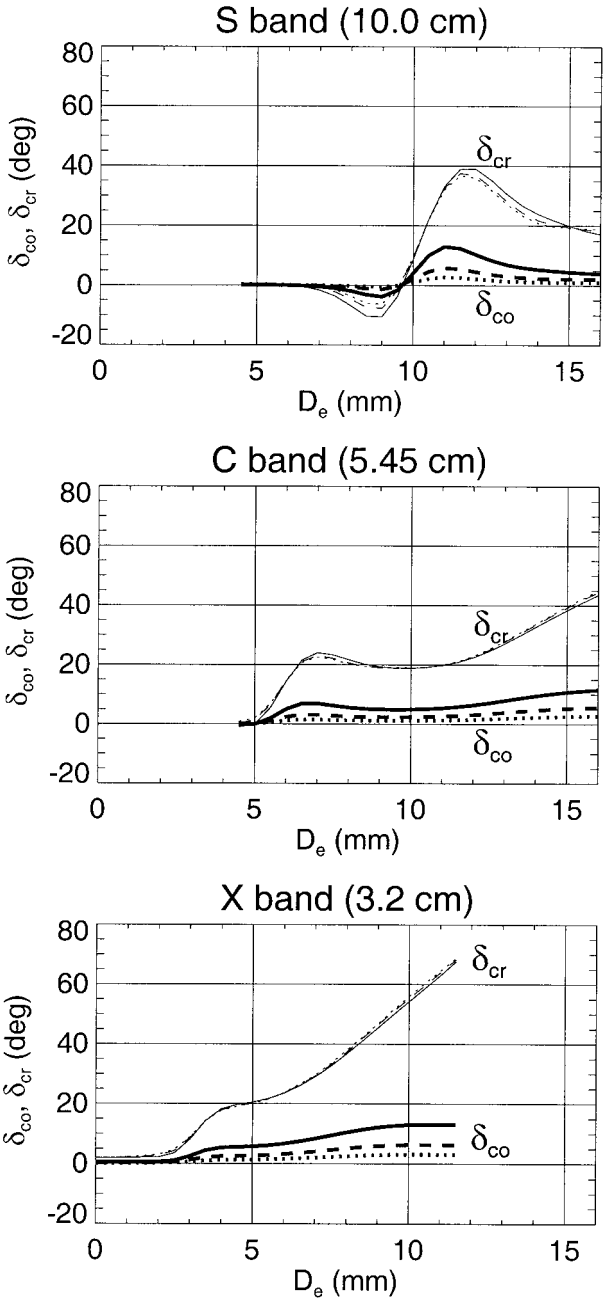


FIG. 7. Dependencies of backscatter differential phase $\delta_{co}$ and depolarization phase $\delta_{cr}$ on equivolume diameter of oblate spheroid with refractive index of water and aspect ratios 0.8 (solid curves), 0.90 (dashed curves), and 0.95 (dotted curves) at (a) S band, (b) C band, and (c) X band.

Both the backscatter differential phase and the depolarization phase depend on a refractive index of scatterers. Generally, the transition between Rayleigh and non-Rayleigh regions on the $D_e$ axis is governed by the parameter $D_e\mathrm{Re}(n)/\lambda$, where n is a complex refractive index. Thus, at a given radar wavelength $\lambda$, the onset of the non-Rayleigh mode of scattering, for which $\delta_{co}$ and $\delta_{cr}$ become essentially different from zero, takes place at smaller sizes of water-coated hailstones than, for example, wet snowflakes because both real and imaginary parts of a refractive index of wet snow are lower than those of water. Magnitudes of $\delta_{co}$ and $\delta_{cr}$ decrease as Im($n$) decreases. Therefore, for wet snow, the curves in Fig. 7 will be shifted towards larger particle sizes and will have shallower extrema. For dry snow, the phases $\delta_{co}$ and $\delta_{cr}$ are very close to zero regardless of size. Hence, discrimination between wet and dry large snowflakes, in principle, is possible with the use of the depolarization phase. The measurements at shorter wavelength are especially promising because of larger values of the depolarization phase and a broader range of snowflake sizes where a non-Rayleigh type of scattering takes place.

Larger values of the depolarization phase $\delta_{cr}$ combined with the fact that $\delta_{cr}$ is almost independent of particle shape and is not affected by particle orientation habit make $\delta_{cr}$ a more attractive polarimetric variable to measure than the backscatter differential phase $\delta_{co}$. Reliable estimates of the depolarization phase, however, can be a problem in the linear polarization basis if pronounced propagation effects are present because the phases of the co–cross-polar correlation coefficients $\rho_{xh}$ and $\rho_{xv}$ become very noisy (Figs. 4, 5). Careful analysis of observational data is required to assess practical use of the depolarization phase measurements. The phases of the co–cross-polar correlation coefficients $\rho_{xr}$ and $\rho_{xl}$ measured in the circular polarization basis are less noisy but are also heavily biased by propagation effects that cannot be easily taken into account. Nevertheless, the depolarization phase is an attractive parameter from the point of view of possible hail detection and sizing, so that any efforts to estimate it unambiguously will be rewarding.

## 5. Summary and conclusions

In this paper, a relatively simple model of the radar scattering by atmospheric particles is used to help interpret all elements of the covariance scattering matrix. The components of the covariance scattering matrix and corresponding polarimetric measurands can be expressed via a limited number of integral parameters that characterize distributions of sizes, shapes, and orientations of meteorological scatterers. For most practically significant cases, a 2D Gaussian distribution of canting angles is sufficient to model orientation of scatterers.

The co–cross-polar correlation coefficients $\rho_{xh}$ and $\rho_{xv}$ measured in the horizontal–vertical (HV) linear polarization basis are the major focus of this study; these polarimetric variables have never been thoroughly explored. It is shown that the magnitudes of $\rho_{xh}$ and $\rho_{xv}$ are determined primarily by the parameters of the canting angle distribution, namely, an absolute value of the mean canting angle $|\langle\alpha\rangle|$ and the rms width of the canting angle distribution $\sigma$. In a special case of raindrops that have direction of their symmetry axis narrowly distributed around the vertical, the magnitudes of $\rho_{xh}$ and $\rho_{xv}$ are roughly proportional to the ratio $|\langle\alpha\rangle|/\sigma$. This is in contrast to the magnitudes of the co–cross-polar correlation coefficients $\rho_{xr}$ and $\rho_{xl}$ measured in the circular polarization basis (known as ORTT) that do not depend on the mean canting angle and are less sensitive to the $\sigma$ variations in rain.

In the absence of propagation effects, the phases of $\rho_{xh}$ and $\rho_{xv}$ are very close to either 0 or $\pm\pi$ for Rayleigh scatterers, depending on the sign of the mean canting angle $\langle\alpha\rangle$ in the radar resolution volume. Under the same conditions, the arguments of $\rho_{xr}$ and $\rho_{xl}$ are equal to $\pm 2\langle\alpha\rangle$. An additional term in the phase of the co–cross-polar correlation coefficients (the so-called depolarization phase) is present if the scatterers are non-Rayleigh. Depolarization phase $\delta_{cr}$ is potentially a very attractive polarimetric parameter that can be used for detection and sizing of melting hail and for discrimination between wet and dry snow. The phase $\delta_{cr}$ is significantly larger than the backscatter differential phase $\delta_{co}$, that is, the argument of the co–polar correlation coefficient $\rho_{hv}$. Another advantage of the depolarization phase is that it is almost insensitive to the hydrometeor shape and is not affected by the type of particle orientation whereas $\delta_{co}$ tends to zero for quasispherical or randomly oriented scatterers.

A model of the mean canting angle varying along a propagation path was developed to examine effects of propagation on the co–cross-polar correlation coefficients. We show that the magnitudes of $\rho_{xh}$ and $\rho_{xv}$ experience pronounced trend with distance if the mean canting angle averaged over a long propagation path (i.e., ''net'' canting angle) is different from zero by a degree or even tenths of a degree. The same type of trend is expected due to antenna feed horn misalignment, nonorthogonality of the ''*H*'' and ''*V*'' waves, etc. Thus, the analysis of the $|\rho_{xh,xv}|$ trends, with distance in relatively uniform precipitation, can serve as a quality check for antenna and microwave assembly imperfections and as a tool to validate simultaneous scheme of transmission/reception that is going to be employed on the WSR-88D radar because the performance of the simultaneous scheme depends crucially on the net canting angle (Doviak et al. 2000). Our preliminary analysis of the data collected with the S-Pol dual-polarization radar (Ryzhkov et al. 2000) did not reveal pronounced trends in the magnitudes of $\rho_{xh}$ and $\rho_{xv}$—an indication that in reality, the net canting angle is close to zero within a few tenths of a degree. This, however, requires more scrutiny.

If the net canting angle is close to zero, then the magnitudes of $\rho_{xh}$ and $\rho_{xv}$ are not biased by propagation effects and can be used to estimate the parameters of the canting angle distribution $|\langle\alpha\rangle|$ and $\sigma$. We derived formulas (35)–(37) that can be used for $|\langle\alpha\rangle|$ and $\sigma$ retrieval in rain medium. Knowledge of the width of the canting angle distribution $\sigma$ is essential in order to assess the performance of the polarimetric rainfall algorithm that is based on specific differential phase. Noticeable rainfall underestimation is expected for $\sigma$ exceeding 15°–20°.

Major theoretical conclusions in this paper regarding behavior of the co–cross-polar correlation coefficients measured in the HV basis are used to explain observational data reported by Ryzhkov et al. (1999, 2000).

*Acknowledgments.* I am grateful to Drs. D. Zrnić and R. Doviak who read the paper and made very useful comments. Discussions with Drs. V. Bringi, J. Hubbert, and J. Vivekanandan also helped to clarify the main ideas presented in this study. I am especially thankful to Dr. S. Matrosov, whose critical remarks allowed me to unveil the error in the computer code that deals with accounting for propagation effects.

## APPENDIX

### Angular Moments

Here we present analytical formulas for the angular moments defined by (13) for three special cases.

*a. Fully chaotic orientation of hydrometeors*

$$A_1 = A_2 = \frac{1}{3}, \qquad A_3 = A_4 = \frac{1}{5}, \qquad A_5 = \frac{1}{15},$$
$$A_6 = A_7 = A_8 = 0, \qquad B_1 = \frac{2}{3}, \qquad B_2 = \frac{8}{15},$$
$$B_3 = B_4 = B_5 = 0. \tag{A1}$$

*b. Random orientation in the horizontal plane*

This orientation is typical for columnar type crystals, which tend to be oriented with their major dimensions in the horizontal plane.

$$A_1 = \frac{1}{2}\sin^2\beta, \qquad A_2 = \frac{1}{2}, \qquad A_3 = \frac{3}{8}\sin^4\beta,$$
$$A_4 = \frac{3}{8}, \qquad A_5 = \frac{1}{8}\sin^2\beta,$$
$$A_6 = A_7 = A_8 = 0, \qquad B_1 = \frac{1}{2}(1 + \sin^2\beta),$$
$$B_2 = \frac{3}{8} + \frac{1}{4}\sin^2\beta, \qquad B_3 = \frac{1}{2}(\sin^2\beta - 1),$$
$$B_4 = \frac{3}{8}(\sin^4\beta - 1),$$
$$B_5 = \frac{3}{8} - \frac{3}{4}\sin^2\beta + \frac{3}{8}\sin^4\beta. \tag{A2}$$

In (A2), $\beta$ is the elevation angle of the radar beam (Fig. 1).

*c. Two-dimensional axisymmetric Gaussian distribution of orientations*

If angle $\langle\psi\rangle$ is not very close to zero and the width of angular distribution is not very large, then axisymmetric Gaussian distribution of orientation can be approximated by the formula

$$p(\psi, \alpha) = \frac{1}{2\pi\sigma\sigma_\alpha}\exp\left[-\frac{(\psi - \langle\psi\rangle)^2}{2\sigma^2} - \frac{(\alpha - \langle\alpha\rangle)^2}{2\sigma_\alpha^2}\right], \tag{A3}$$

where the angles $\langle\psi\rangle$ and $\langle\alpha\rangle$ determine the mean orientation of particles and parameters $\sigma$ and $\sigma_\alpha = \sigma/\sin\langle\psi\rangle$ define the width of the angular distribution along $\psi$ and $\alpha$ directions, respectively (see Fig. 1) This type of angular distribution represents a wide class of atmospheric scatterers that can be modeled as oblate spheroids, including raindrops, snowflakes, graupel, and hail. Approximation (A3) allows us to perform averaging over angles $\psi$ and $\alpha$ independently, and the angular moments $A_i$ and $B_i$ can be expressed as the products of the following factors:

$$\langle\sin^2\psi\rangle = \frac{1}{2}(1 - r\cos2\langle\psi\rangle),$$
$$\langle\sin^4\psi\rangle = \frac{3}{8} - \frac{1}{2}r\cos2\langle\psi\rangle + \frac{1}{8}r^4\cos4\langle\psi\rangle,$$
$$\langle\cos^2\alpha\rangle = \frac{1}{2}(1 + r_\alpha\cos2\langle\alpha\rangle),$$
$$\langle\sin^2\alpha\rangle = \frac{1}{2}(1 - r_\alpha\cos2\langle\alpha\rangle),$$
$$\langle\cos^4\alpha\rangle = \frac{3}{8} + \frac{1}{2}r_\alpha\cos2\langle\alpha\rangle + \frac{1}{8}r_\alpha^4\cos4\langle\alpha\rangle,$$
$$\langle\sin^4\alpha\rangle = \frac{3}{8} - \frac{1}{2}r_\alpha\cos2\langle\alpha\rangle + \frac{1}{8}r_\alpha^4\cos4\langle\alpha\rangle,$$
$$\langle\cos^2\alpha\sin^2\alpha\rangle = \frac{1}{8}(1 - r_\alpha^4\cos4\langle\alpha\rangle),$$

$$\langle \sin 2\alpha \rangle = r_\alpha \sin 2\langle \alpha \rangle,$$

$$\langle \cos^2\alpha \sin 2\alpha \rangle = \frac{1}{2} r_\alpha \sin 2\langle \alpha \rangle + \frac{1}{4} r_\alpha^4 \sin 4\langle \alpha \rangle,$$

$$\langle \sin^2\alpha \sin 2\alpha \rangle = \frac{1}{2} r_\alpha \sin 2\langle \alpha \rangle - \frac{1}{4} r_\alpha^4 \sin 4\langle \alpha \rangle,$$

$$\langle e^{\pm j2\alpha} \rangle = r_\alpha e^{\pm j2\langle \alpha \rangle}, \qquad \langle e^{j4\alpha} \rangle = r_\alpha^4 e^{j4\langle \alpha \rangle}, \tag{A4}$$

where $r = \exp(-2\sigma^2)$ and $r_\alpha = \exp(-2\sigma_\alpha^2)$.

## REFERENCES


Antar, Y. M. M., and A. Hendry, 1987: Correlation techniques in two-channel linearly polarized radar systems. *Electromagnetics,* **7,** 17–27.

Aydin, K., and T. A. Seliga, 1984: Radar polarimetric backscattering properties of conical graupel. *J. Atmos. Sci.,* **41,** 1887–1892.

Balakrishnan, N., and D. S. Zrnić, 1990: Use of polarization to characterize precipitation and discriminate large hail. *J. Atmos. Sci.,* **47,** 1525–1540.

Beard, K. V., and A. R. Jameson, 1983: Raindrop canting. *J. Atmos. Sci.,* **40,** 448–454.

Brandes, E. A., A. V. Ryzhkov, and D. S. Zrnić, 2001: An evaluation of radar rainfall estimates from specific differential phase. *J. Atmos. Oceanic Technol.,* **18,** 363–375.

Bringi, V. N., and A. Hendry, 1990: Technology of polarization diversity radars for meteorology. *Radar in Meteorology,* D. Atlas, Ed., Amer. Meteor. Soc., 153–190.

——, V. Chandrasekar, N. Balakrishnan, and D. S. Zrnić, 1990: An examination of propagation effects on radar measurements at microwave frequencies. *J. Atmos. Oceanic Technol.,* **7,** 829–840.

Brunkow, D. A., P. C. Kennedy, S. A. Rutledge, V. N. Bringi, and V. Chandrasekar, 1997: CSU-CHILL radar status and comparison of available operating modes. Preprints, *28th Conf. on Radar Meteorology,* Austin, TX, Amer. Meteor. Soc., 43–44.

Caylor, I. J., and V. Chandrasekar, 1996: Time-varying ice crystal orientation in thunderstorms observed with multiparameter radar. *IEEE Trans. Geosci. Remote Sens.,* **34,** 847–858.

Doviak, R. J., V. N. Bringi, A. V. Ryzhkov, A. Zahrai, and D. S. Zrnić, 2000: Considerations for polarimetric upgrades to operational WSR-88D radars. *J. Atmos. Oceanic Technol.,* **17,** 257–278.

Hendry, A., Y. M. M. Antar, and G. C. McCormick, 1987: On the relationship between the degree of preferred orientation in precipitation and dual-polarization radar echo characteristics. *Radio Sci.,* **22,** 37–50.

Holt, A. R., 1984: Some factors affecting the remote sensing of rain by polarization diversity radar in the 3-to 35-GHz frequency range. *Radio Sci.,* **19,** 1399–1412.

——, and J. W. Shepherd, 1979: Electromagnetic scattering by dielectric spheroids in the forward and backward directions. *J. Phys. A Math. Gen.,* **12,** 159–166.

——, V. N. Bringi, and D. Brunkow, 1999: A comparison between parameters obtained with the CSU-CHILL radar from simultaneous and switched transmission of vertical and horizontal polarization. Preprints, *29th Int. Conf. on Radar Meteorology,* Montreal, PQ, Canada, Amer. Meteor. Soc., 214–217.

Hubbert, J. C., V. N. Bringi, and G. Huang, 1999: Construction and interpretation of S-band covariance matrices. Preprints, *29th Int. Conf. on Radar Meteorology,* Montreal, PQ, Canada, Amer. Meteor. Soc., 205–207.

Jameson, A. R., 1985: Deducing the microphysical character of precipitation from multiple-parameter radar polarization measurements. *J. Climate Appl. Meteor.,* **24,** 1037–1047.

——, 1987: Relations among linear and circular polarization parameters measured in canted hydrometeors. *J. Atmos. Oceanic Technol.,* **4,** 634–645.

Krehbiel, P., T. Chen, S. McCrary, W. Rison, G. Gray, and M. Brook, 1996: The use of dual-channel circular-polarization radar observations for remotely sensing storm electrification. *Meteor. Atmos. Phys.,* **59,** 65–82.

Lutz, J., B. Rilling, J. Wilson, T. Weckwerth, and J. Vivekanandan, 1997: S-Pol after three operational deployments, technical performances, sitting experiences, and some data examples. Preprints, *28th Conf. on Radar Meteorology,* Austin, TX, Amer. Meteor. Soc., 286–287.

Matrosov, S. Y., R. F. Reinking, R. A. Kropfli, and B. W. Bartram, 1996: Estimation of ice hydrometeor types and shapes from radar polarization measurements. *J. Atmos. Oceanic Technol.,* **13,** 85–96.

McCormick, G. C., and A. Hendry, 1974: Polarization properties of transmission through precipitation over a communication link. *J. Rech. Atmos.,* **8,** 175–187.

——, and ——, 1975: Principles for radar determination of the polarization properties of precipitation. *Radio Sci.,* **10,** 421–434.

Metcalf, J. I., 1988: A new slant on the distribution and measurement of hydrometeor canting angles. *J. Atmos. Oceanic Technol.,* **5,** 571–578.

Oguchi, T., 1983: Electromagnetic wave propagation and scattering in rain and other hydrometeors. *Proc. IEEE,* **71,** 1029–1078.

Olsen, R. L., 1981: Cross-polarization during precipitation on terrestrial links: A review. *Radio Sci.,* **16,** 761–779.

Pruppacher, H. R., and R. L. Pitter, 1971: A semi-empirical determination of the shape of cloud and rain drops. *J. Atmos. Sci.,* **28,** 86–94.

Ryzhkov, A. V., 1991: Polarimetric information measurements in radar meteorology. Theoretical model (in Russian). *Radioelectron. Commun. Syst.,* **2,** 17–23.

——, and D. S. Zrnić, 1996: Assessment of rainfall measurement that uses specific differential phase. *J. Appl. Meteor.,* **35,** 2080–2090.

——, ——, V. N. Bringi, G. Huang, E. A. Brandes, and J. Vivekanandan, 1999: Characteristics of hydrometeor orientation obtained from radar polarimetric measurements in a linear polarization basis. *Proc. IGARSS '99,* Hamburg, Germany, IEEE, 702–704.

——, ——, J. C. Hubbert, V. N. Bringi, J. Vivekanandan, and E. A. Brandes, 2000: Interpretation of polarimetric radar covariance matrix for meteorological scatterers. *Proc. IGARSS 2000,* Honolulu, HI, IEEE, 1584–1586.

Sachidananda, M., and D. S. Zrnić, 1986: Differential propagation phase shift and rainfall rate estimation. *Radio Sci.,* **21,** 235–247.

Saunders, M. J., 1971: Cross-polarization at 18 and 30 Ghz due to rain. *IEEE Trans. Antennas Propag.,* **AP19,** 273–277.

Seliga, T. A., and V. N. Bringi, 1976: Potential use of radar differential reflectivity measurements at orthogonal polarizations for measuring precipitation. *J. Appl. Meteor.,* **15,** 69–76.

Straka, M. J., and D. S. Zrnić, 1993: An algorithm to deduce hydrometeor types and contents from multiparameter radar data. Preprints, *26th Int. Conf. on Radar Meteorology,* Norman, OK, Amer. Meteor. Soc., 513–515.

Torlaschi, E., and A. R. Holt, 1993: Separation of propagation and backscattering effects in rain for circular polarization diversity S-band radars. *J. Atmos. Oceanic Technol.,* **10,** 465–477.

——, and ——, 1998: A comparison of different polarization schemes for the radar sensing of precipitation. *Radio Sci.,* **33,** 1335–1352.

Ulbrich, C. W., 1983: Natural variations in the analytical form of the raindrop size distributions. *J. Appl. Meteor.,* **22,** 1764–1775.

Vivekanandan, J., W. M. Adams, and V. N. Bringi, 1991: Rigorous approach to polarimetric radar modeling of hydrometeor orientation distributions. *J. Appl. Meteor.,* **30,** 1053–1063.

——, D. S. Zrnić, S. M. Ellis, R. Oye, A. V. Ryzhkov, and J. Straka, 1999: Cloud microphysics retrieval using S-band dual-polarization radar measurements. *Bull. Amer. Meteor. Soc.,* **80,** 381–388.

Zrnić, D. S., 1991: Complete polarimetric and Doppler measurements with a single receiver radar. *J. Atmos. Oceanic Technol.,* **8,** 159–165.

——, and A. V. Ryzhkov, 1999: Polarimetry for weather surveillance radars. *Bull. Amer. Meteor. Soc.,* **80,** 389–406.